Journal of Materials Chemistry A

Accepted Manuscript

ROYAL SOCIETY OF CHEMISTRY

www.rsc.org/materialsA

Journal Name

ARTICLE

Enhanced Electrocatalytic Activity of Gold Nanoparticles on Hydroxyapatite Nanorods for Sensitive Hydrazine Sensors

Received 00th January 20xx,
Accepted 00th January 20xx

DOI: 10.1039/x0xx00000x

www.rsc.org/

G. Bharath,[a,b]* Alberto Naldoni,[c] K. Hasini Ramsait, [b] Ahmed Abdel-Wahab,[d] Rajesh Madhu, [e] Edreese Alsharaeh [a]* and N. Ponpandian[b]*

Abstract

Well-designed noble metals and ceramic nanoarchitectures are significantly important for the development of high performance, selective, sensitive and cost effective electrochemical sensors. Here, we report gold (Au) nanoparticles (NPs) uniformly dispersed on hydroxyapatite (HAp) nanorods forming particles on rods nanoarchitectures for sensitive hydrazine sensors. The Au/HAp nanocomposites were prepared by a versatile hydrothermal-precipitation method. The precipitated citrate-stabilized Au NPs were 6-8 nm in size and strongly anchored onto rod-shaped HAp with a diameter of 10 nm and length of 65 nm. The structural, chemical, electrochemical properties and growth mechanism of the Au nanoparticles onto the HAp nanorods (NRs) is presented. Progress toward the application of hybrid nanocomposites in electrochemical oxidation of hydrazine is overviewed. Compared to Au NPs, the incorporation of Au NPs into HAp NRs favored the adsorption of hydrazine, thus bringing hydrazine very closer to the catalytic sites of Au NPs and then increasing the efficiency of hydrazine oxidation in neutral solution. The amperometric (*i-t*) hydrazine sensor, using the as-prepared Au/HAp as the electrochemical catalyst, shows a wide linear response range of 0.5-1429 µM, a lower detection limit (0.017 µM) and very high sensitivity of 0.5 $\mu A \mu M^{-1} cm^{-2}$. Furthermore, the Au/HAp nanocomposites showed an excellent anti-interference property towards the various organic and inorganic electroactive compounds, and good inter-electrode and intra-electrode reproducibility. Our present technique shows both qualitative and quantitative measurement of hydrazine in various water samples with high sensitivity, cost effective and rapid analysis time.

1. Introduction

Recently, the current research has been focused on the development of efficient heterogeneous electrocatalysts possessing higher electrochemical activity towards the sensing of many organic and inorganic compounds with highly selective, sensitive and stable sensing platforms. Nanostructured metal particles (Au, Pd and Pt) play a vital role in catalytic and electrocatalytic reactions, especially in sensing platforms.[1] Nanosized gold (Au) particles are of increasing significance in various fields such as sensors, catalysis, biomedical, microelectronics and biological recognition.[2] For instance, Au nanoparticles (NPs) supported on an metal oxides and metal hydroxides ($Mg(OH)_2$ and MgO) surface show very high catalytic activity toward carbon monoxide (CO) oxidation and it has attracted the highest interest and is the most extensively studied on.[3] Recently, Au supported metaloxides, polymers, graphene and ceramic nanocomposites have been used as nanoscale electrocatalysts for constructing the catalytic nano interfaces of electronic devices to achieve high-sensitive and selective electrochemical sensors. Specifically, Au@Fe_3O_4, Au@α-Fe_2O_3, Au@ZnO, Au@Graphene, Au@molecularly imprinted polymers, Au@hydroxyapatite@chitosan and Au@activated carbon have recently been applied in a high efficient electrodes to detect various organic and inorganic compounds.[4-10] Such structures have some inherent drawbacks such as electrode pulverization, high overpotential, corrosion and poor electrode sturdy when used as a catalyst substrate.

On the other hand hydroxyapatite ($Ca_{10}PO_6(OH)_2$, HAp), a kind of inorganic mesoporous material, has attracted potential value for high biocompatibility, surface area and excellent adsorption property, which have been widely used as drug carrier, implant material, bone fillers, adsorbent, photocatalyst and electrochemical sensors.[11-13] In particular, HAp modified electrodes have attracted much attention mainly attributed to detection kidney injury molecule 1 (KIM-1), uric acid, 4-

[a] Department of Chemistry, Alfaisal University, P.O. Box 50927, Riyadh 11533, Saudi Arabia. E-mail: sribharath7@gmail.com, ealsharaeh@alfaisal.edu
[b] Department of Nanoscience and Technology, Bharathiar University, Coimbatore 641 046, India. E-mail: ponpandian@buc.edu.in
[c] CNR–Istituto di Scienze e Tecnologie Molecolari, Via C. Golgi 19, 20133 Milano, Italy
[d] Chemical Engineering Program, Texas A&M University at Qatar, P.O. Box 23874, Doha, Qatar.
[e] Department of Chemical Engineering and Biotechnology, National Taipei University of Technology, Taipei 10608, Taiwan.

nitrophenol, ltyrosine, hemoglobin (Hb) and glucose molecules.[14-19] Interestingly, electrochemical property is strongly depends on the crystallinity, dimensional anisotropy and morphology of the HAp nanocrystals for essential constructive applications.[20,21] HAp nanorods (NRs) exhibit a small dimensions, good crystallinity and high surface area which have shown to be an excellent electrochemical activity. Many researchers have been devoted to the design and synthesis of 1D HAp using some additives such as phosphorus-containing biomolecules and organic molecules through hydrothermal techniques.[22-26] Adenosine 5'-triphosphate (ATP) is the most common phosphorus-containing biomolecules and it was used as a phosphorus source to synthesis 1D HAp by a hydrothermal method. The obtained 1D HAp has good crystallinity, high specific surface area (SSA) possesses higher electrochemical active sites toward the sensing of various organic compounds.[22,19]

Despite a growing research effort, however, electrocatalysts design remains an important challenge to improve the electrochemical performance, solving the electrode pulverization problem and keep the overall electrode sturdy. HAp and Au based electrocatalysts are well studied and among the most efficient for electrochemical sensors. In recent years, Au NPs supported on metal oxides and or carbon materials have been shown to be attractive electrocatalysts in a number of selective oxidation of hydrazine, 4-nitrophenol, glucose, uric and ascorbic acids. More recently, very few researchers were developed hemoglobin immobilized Au/HAp, Au-HAp-chitosan film and Au/FeOx-HAp has been developed for the detection of hydrogen peroxide (H_2O_2), tandem catalysis, immunosensor and CO oxidation.[27-30] Prior to this work, there have been no examples in the literature of high sensitive and selective Au/HAp sensor for the detection of hydrazine. Hydrazine (N_2H_4) is of practical interest due to its wide application in fuel for satellites and rockets, photographic chemicals, insecticides, emulsifiers, plastic blowing agent, textile dyes, and anticorrosion agent for nuclear and electrical power plants. Despite its common use, hydrazine is rather toxic, colorless, and flammable, which can severely injury liver, lungs, brain, kidneys, and spinal cord. As a result, an accurate determination of trace level hydrazine through electrochemical method is of great relevance. Electrochemistry is an important approach to determine the hydrazine at trace level and it exhibits high sensitivity and selectivity, simplicity, and low cost.[31-33] However, an electrochemical sensor desires high-performance electrocatalysts. The Au/HAp is currently of interest as the electrocatalyst due to its high catalytic activity, sensitivity, selectivity, and low overpotential toward hydrazine oxidation, which is the focus of this paper.

Herein, we prepare Au NPs on HAp NRs (particles on rods nanoarchitectures) as high performance electrode toward the sensitive detection of hydrazine. A possible nucleation growth mechanism was proposed for HAp NRs and Au NPs on them. The glassy carbon electrode (GCE) modified with this Au/HAp nanocomposites exhibits admirable electrocatalytic activity to construct sensitive sensor for the electrochemical detection of hydrazine. The fabricated Au/HAp nanocomposite modified GCE detects hydrazine at a lower overpotential (0.15 V) with high sensitivity than that of Au/GCE, and bare GCE. An Au/HAp rotating disk electrode (RDE) was fabricated and used to detect trace level hydrazine in various water source such as lake, river and tap water. The present high performance electrode provides high sensitivity, selectivity and lower detection limit toward the detection of hydrazine.

2. Experimental

2.1 Materials

Adenosine 5′-triphosphate disodium salt hydrate ($C_{10}H_{14}N_5Na_2O_{13}P_3 \cdot xH_2O$), calcium chloride dihydrate ($CaCl_2.2H_2O$), sodium citrate and $HAuCl_4 \cdot 3H_2O$ were purchased from Sigma-Aldrich. Ammonium hydroxide (NH_4OH), acetone and ethanol were purchased from Himedia, India. All the reagents and chemicals were used without further purification.

2.2 Synthesis of 1D hydroxyapatite (HAp) nanorods via hydrothermal process.

The 1D HAp was prepared by hydrothermal synthesis route by using $ATPNa_2$ as an organic phosphate source. In a typical synthesis procedure, 44 mg of $CaCl_2.2H_2O$ dissolved in 10 mL of water was the solution A, while solution B was formed by 30 mg of $ATPNa_2$ dissolved in 10 mL of water. Consequently, solution B ($ATPNa_2$) was added drop wise to solution A and pH was adjusted to10.5 by adding an ammonium hydroxide solution (30%) under vigorous stirring for 30 min. Finally, the mixed solution was transferred to the Teflon-lined stainless steel autoclave. The autoclave was put in an oven at 180 ^oC for 12 h and slowly cooled down to room temperature naturally. The white color precipitate was washed several times with ethanol and water. Finally, the resulting product was dried at 70 ^oC under a vacuum.

2.3 Synthesis of Au NPs / 1D HAp NRs via simple precipitation process.

In a typical experiment for the preparation of Au NPs grown on 1D HAp NRs, 0.25 g of $HAuCl_4 \bullet 3H_2O$ and 24 mg of sodium citrate was dissolved in 10 mL deionized water. Afterwards, the reaction mixture was maintained at the boiling temperature till a ruby-red color appeared, resulting Au colloidal solution were obtained. Meanwhile, 100 mg of as-prepared HAp NRs were dispersed in 30 mL of ethanol to form stable white color solution. Subsequently, Au colloidal solution was added to the NRs solution with constant stirring and heated at 80 ^oC for 15 min. After cooled at room temperature, the samples were washed with deionized water and dried at 60 ^oC in vacuum.

2.3 Characterization

The morphology of the HAp and Au/HAp samples were observed by field emission scanning electron microscopy (FESEM) (FEI Quanta-250 FEG) coupled with EDX spectroscopy. The X-ray diffraction (XRD) measurements were carried out at room temperature using a PAN analytical (X-Pert-Pro) diffractometer with a Cu $K\alpha_1$ radiation (λ= 1.5406 Å)

over a scanning interval (2θ) from 10 to 70°. The average crystallite sizes of HAp and Au/HAp NRs were estimated using the Scherrer formula by using the X-ray line broadening. The infrared spectrum of the samples was obtained by using a Fourier transform infrared (FTIR) spectrometer (Bruker Tensor 27, Germany). The sample was prepared by a KBr pellet by investigating the peaks within the range of 4000 to 450 cm^{-1}. The specific surface areas and pore sizes were determined by BET-N_2 adsorption for the Au/HAp nanocrystals using a micromeritics ASAP 2020 surface area analyzer.

2.4 Fabrication of Au/HAp/GCE nanocomposite modified GCE

GCE was polished before each experiment with 1, 0.3 and 0.05 mm alumina powder and then rinsed thoroughly with distilled water and ultrasonicated in an alcoholic solution. The cleaned GCE was dried with pure nitrogen atmosphere and treated by dropping a suspension (6μL) of Au/HAp/GCE nanocomposites in ethanol (2 mg/L) on it and followed by drying in a hot air oven at 30 °C for 30 min. Then the Au/HAp/GCE modified GCE was gently rinsed few times with double distilled water to remove the loosely bound Au/HAp/GCE. Similar procedure was also followed to prepare Au/RGO modified GCE.

3. Results and Discussion

3.1. Nucleation growth mechanism

The formation mechanism of Au NPs dispersed on highly *c-axis* oriented one dimensional (1D) HAp NRs are shown in Scheme 1. The Au/HAp nanocomposites were prepared by two step hydrothermal crystalization process. Firstly, well dispersed and high crystallinity HAp NRs were prepared via hydrothermal process at 180 °C for 12 h with adenosine 5'-triphosphate disodium salt (ATP) as the phosphorus source and stabilizer. Secondly, Au NPs grown on 1D HAp NRs were prepared via simple precipitation process at 60 °C for 6 h by addition of certain molar ratio Au^{3+}-citrate solutions.

The formation mechanism of 1D HAp NRs was proposed based on the present experimental results and already available literature. The schematic illustration for the hydrothermal synthesis of HAp NRs is shown in Step-I. ATP was the organic phosphate (PO_4^{3-}) sources for preparation of well dispersed HAp NRs. The growth mechanism is composed of two stages: during the first step, ATP molecules were hydrolyzed to gradually release inorganic phosphate ions (PO_4^{3-}) under a hydrothermal temperature. Gradually released PO_4^{3-} ions reacted with Ca^{2+} ions via electrovalent bonds and pH was adjusted, resulting in the formation of HAp nuclei. In second stage, hydrothermal temperature played a vital role to improve the crystallinity and orientational growth of HAp. On the other hand, the Au NPs were grown on 1D HAp NRs via simple precipitation process at 60 °C for 6 h.

Detailly, as-prepared 1D HAp NRs were dispersed in ethanol and gold colloidal solution was prepared by the citrate reduction of $HAuCl_4$. A possible reaction mechanism (Step-II) in order to describe the reduction of Au(III) by sodium citrate. In a typical citrate reduction process, Au(III) turn to Au(I) and further it was reduces by citrate ions to be formed metallic Au(0). The reaction mechanism of Au colloids formation, surface charges and sizes is dependent on the concentration of the citrate ions ($C_6H_5O_7^{3-}$) and $HAuCl_4$. The overall chemical reaction mechanism can be presented as

$$Au^{3+} + C_6H_5O_7^{3-} + 15OH^- \rightarrow Au + 6CO_2 + 10H_2O \quad (1)$$

Moreover, surfaces of Au NPs are covered with the negatively charged OH^- ions that causes the particles to repel each other, resulting stable in a colloidal form.

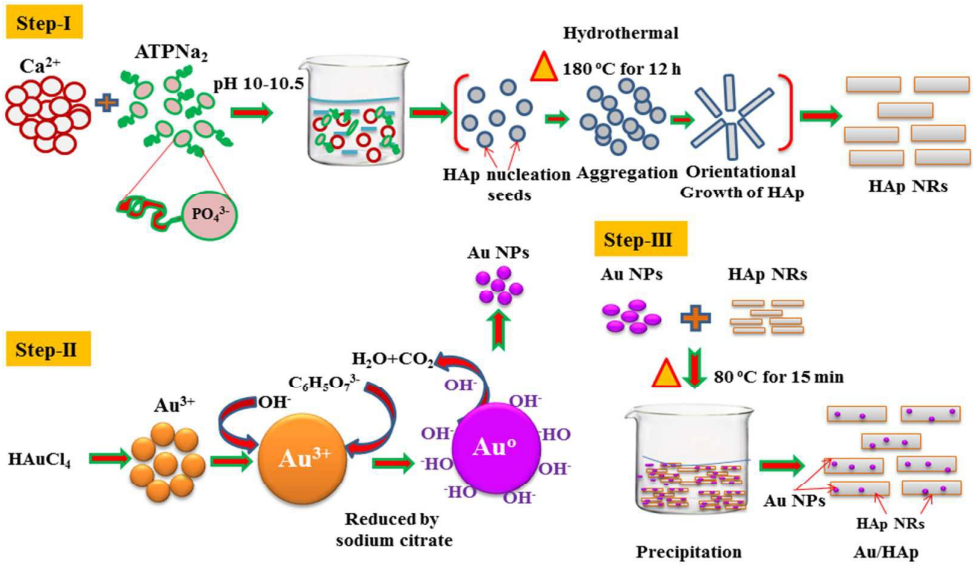

Scheme. 1 Schematic diagrams: Step-I) formation of HAp NRs by a hydrothermal method at 180 °C for 12 hrs using ATP as the phosphorus source, Step-II) formation of citrate capped Au NPs and Step-III) formation of Au NPs on HAp NRs by simple precipitation method.

Further, the OH^- ions covered Au colloids are adsorbed on Ca^{2+} sites on the surfaces of HAp via weak electrostatic interaction and corresponding formation mechanism are shown in Step-III. Basically, hexagonal apatite structure comprises positivelly charged Ca^{2+} sites surrounded by the negatively charged tetrahedral PO_4^{3-} units; OH^- ions occupy columns parallel to the hexagonal axis. Therfore, positively charged Ca^{2+} sites of HAp may be responsible for the attraction of negatively charged Au colloids resulting in Au NPs uniformely dispersed on the surfaces of HAp NRs.

3.2 Physico-chemical properties

To obtain more detailed information about the nanoparticle morphology, composition and crystallinity of the HAp NRs we acquired FESEM, TEM, EDS and SAED pattern. Figure 2 a-d show the FESEM and TEM micrographs of HAp nanostructures. Both analyses reveal that the samples have rods-like morphology and the size of the NRs is approximately 10 nm in width, while the length is ~65 nm. Figure 2 is also reveals well-dispersed and dimensionally monodisperse NRs. The finer morphology of HAp NRs was obtained thanks to the slow release of PO_4^{3-} ions from $ATPNa_2$ and the reaction with Ca^{2+} ions via electrovalent bonds to form HAp nuclei. The slow addition of PO_4^{3-} ions prevents the agglomeration of HAp nuclei, resulting in finer rods-like morphology. Whereas, inorganic phosphate ions are used as the phosphorus source in the preparation of HAp, the supersaturation of Ca^{2+} ions and PO_4^{3-} ions in the precursor solution leads to rapid nucleation growth and a disordered growth of HAp, and the morphology and size of the samples are difficult to control. The selected area electron diffraction (SAED) pattern of the HAp NRs is shown in Figure 2e.

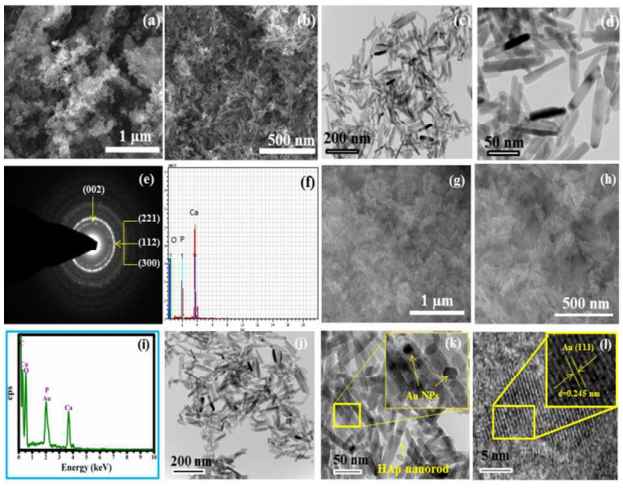

Fig. 2 FESEM (a and b) and TEM (c and d) micrographs with different magnification, SAED pattern (e), EDX (f) analysis of HAp NRs prepared by using $ATPNa_2$ as a phosphorus source at 180 ^oC for 12 h, FESEM (g and h) with EDS spectrum (i), TEM (j and k), HRTEM (l) micrographs with different magnifications for Au in the Au/HAp nanocomposites.

The diffraction rings of (002), (221), (112) and (300) correspond to HAp hexagonal phases. Further, the elemental composition and quantitative analysis of HAp crystallite were analysed from EDS spectrum (Figure 2f). It can be seen that the presence of strong O, Ca and P signals is clearly detected in the EDS spectrum indicating the formation of HAp and no other impurities were detected. A quantitative analysis of the HAp nanocrystallites was carried out from the ratio between Ca and P signals in the EDS spectrum and yielded a Ca:P ratio of 1.64 : 1. This results is in good agreement with the stoichiometry based on the hexagonal structure of HAp $[Ca_{10}PO_6(OH)_2]$.

Au colloidal NPs were dispersed on the HAp NRs and their morphology, crystalline nature and chemical composition were conformed through FESEM, HR-TEM and EDS. Figure 2g,h show the FESEM images of Au NPs dispersed on HAp NRs; however the presence of small Au NPs cannot be observable, considering the FESEM resolution. The FESEM-EDS in Figure 2c provides the clearer information about distribution of elements in the Au/HAp nanocomposites. It indicates that the samples are composed of calcium (Ca), phosphorus (P), oxygen (O) for the HAp template phase and the Au elements for Au NPs on the surface of HAp NRs. Evidence for the presence of Au NPs on HAp NRs were clearly observed from TEM and HR-TEM analysis. The Au NPs with sizes of 8 nm are highly dispersed on the surfaces of HAp NRs as shown in Figure 2j,k. HRTEM images with lattice fringes (Figure 2l) revealed interdistances corresponding to the (111) plane of fcc Au.

The X-ray diffraction (XRD) patterns were used to analyze the crystalline nature and phases of as-prepared HAp NRs and Au/HAp nanocomposites. The XRD pattern of the nanocomposites indicates the presence of both crystalline HAp (JCPDS card: No. 09-0432) and Au (JCPDS no. 4-0784), as shown in Figure 3. The average crystallite size can be calculated via the Scherrer formula, using the full width at half-maximum (fwhm) of the major peaks belonging to HAp and is estimated to be 25 and 27 nm corresponding to HAp NRs and Au/HAp nanocomposites, respectively.

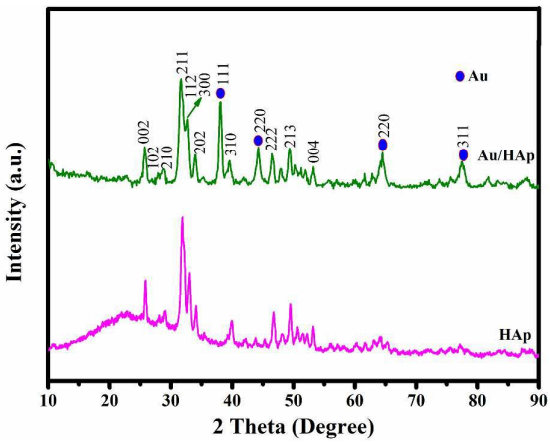

Fig. 3 XRD patterns of the pure HAp and Au/HAp nanocomposite.

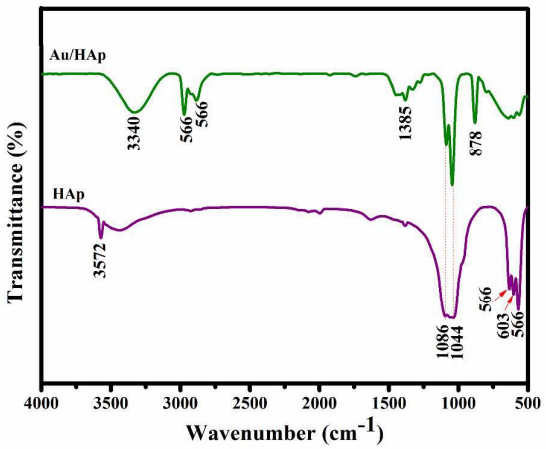

Fig. 4 FTIR spectrum of the pure HAp and Au/HAp nanocomposite

Importantly, these results clearly indicate that the biocompatible $ATPNa_2$ can be used as a new organic phosphate source and stabilizing agent for the synthesis of hexagonal HAp. Furthermore, the presence of structural peaks of cubic Au in XRD patterns and average crystalline size around 8 nm clearly illustrates that Au NPs were synthesized by using sodium citrate with well crystalline nature. As shown in XRD patterns, the addition of Au NPs notably no significant shifting of HAp peak positions, thus signifying that the incorporation of Au NPs does not affect the crystalline nature and phase purity of HAp. These results suggests, the appearance of a well crystallized hexagonal phase of HAp and cubic Au crystal structures were obtained and no other impurity were detected.

The FTIR spectra of HAp NRs and Au/HAp nanocomposites were shown in Figure 4. The characteristic adsorption bands at 566 and 603 cm^{-1} corresponds to the bending vibration (ν_4) of phosphate groups. The (ν_1) vibration of phosphate was observed as a peak at 962 cm^{-1}. The intense bands at 1044 and 1086 cm^{-1} are attributed to the stretching vibration (ν_3) of phosphate groups.[12] The sharp absorption peaks at 3572 and 634 cm^{-1} correspond to the stretching of -OH bands which is confirms that the incorporation of citrate capped Au could not be affect OH site of the HAp. The broad absorption bands around 3447 and 1639 cm^{-1} assigned to OH groups of phenols, alcohols, carboxyl groups and of H_2O of crystallization present in the as-prepared samples. This suggests that there was a no minimal amount of organic residue in the HAp NRs by using $ATPNa_2$ as a phosphorus source under hydrothermal process. Further, the FTIR results confirm, no significant peaks shift was observed by addition of Au in Au/HAp nanocomposite and incorporation of Au NPs does not affect any significant structural changes in HAp.

XPS analysis was used to examine the surface composition of the as-prepared HAp and Au-HAp nanocomposites and the core level spectra (high-resolution XPS spectra of the Ca 2p, P 2p, O 1s, and Au 4f region) are depicted in Figure 5a-e. Besides the expected Ca, P, and O peaks, a small carbon (C 1s) peak was observed at 284.6 eV in all the as-prepared samples. This carbon impurity had atomic percentages changing from 10 to 15 % for HAp and Au-HAp samples and was due to adventitious carbon. The high-resolution XPS scan of the Au 4f region (Figure 5 b) of Au-HAp nanocomposites was separated in two predetermined peaks at 83.7 and 87.0 eV associated to the Au $4f_{7/2}$ and Au $4f_{5/2}$, respectively, typical of metallic Au.[30,34] Figure 5c shows the high-resolution XPS scan of the Ca 2p region represents two peaks for Ca $2p_{1/2}$ and Ca $2p_{3/2}$ at binding energies of 347.5 and 350.4 eV, respectively, which are assigned to calcium phase on HAp.

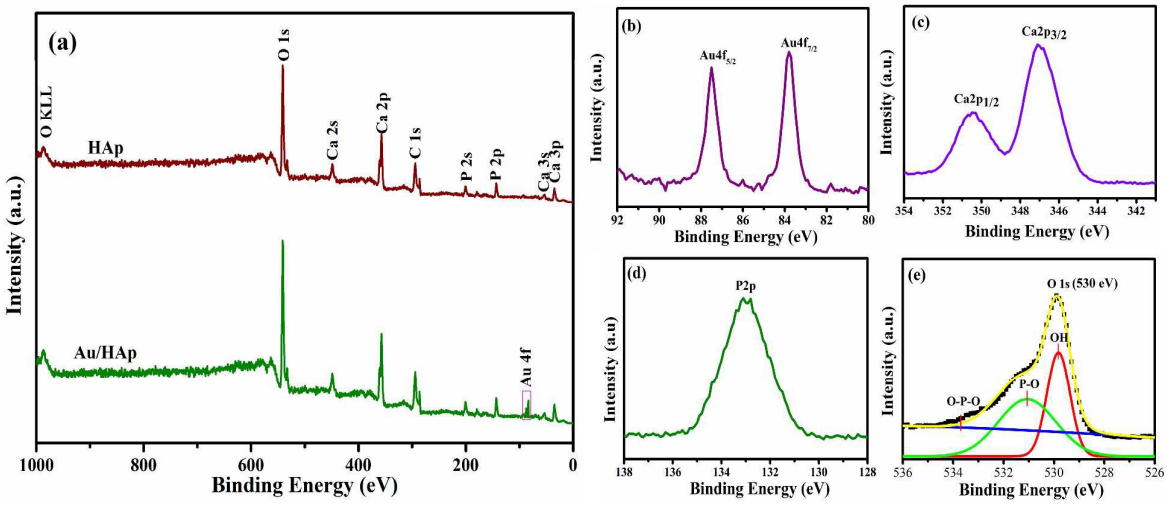

Fig. 5 XPS survey spectra of HAp and Au/HAp nanocomposites (a), high resolution spectra of Au 4f (b), Ca 2p (c), P 2p (d) and O 1s (e).

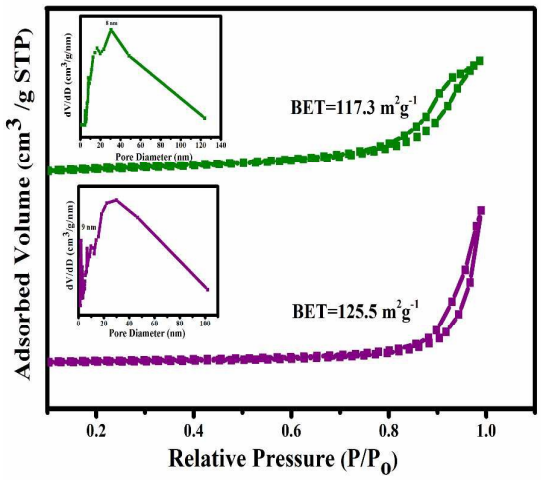

Fig. 6 BET N_2 adsorption/desorption isotherms of (a) HAp NRs and (b) Au/HAp nanocomposites. Inset Figure BJH pore size distributions for (c) HAp NRs and (d) Au/HAp nanocomposites

The high resolution XPS spectrum in Figure 5d shows the peak at 133 eV corresponding to phosphate group (P 2p) in the HAp. The O 1s XPS spectrum (Figure 5e) can be deconvoluted into three distinct peaks due to OH, P-O and P-O-P and having binding energy of 529.8, 531.5 and 533.7 eV, respectively.[19,20]

The textural properties of the HAp and Au/HAp nanocomposites were investigated through BET (Brunauer-Emmett-Teller) surface area analysis and the corresponding N_2 physisorption curves are shown in Figure 6a,b. The N_2 sorption isotherms for both samples exhibit hysteresis loops, which are typical of mesoporous type IV isotherms. The BET specific surface area (SSA) of the as-prepared HAp and AU/HAp nanocomposites was about 125.5 and 117.3 m g^{-1}, respectively. The pore size distributions estimated from the desorption branch of the isotherms based on a BJH (Barret−Joyner−Halenda) model are shown in inset Figure 6. The BJH desorption curves of both samples indicates a broad pore distribution width with an average size centered on 9 ± 1.5 and 8 ± 1.3 nm are corresponds to HAp and Au/HAp nanocomposites, respectively. These results clearly suggest that the higher SSA and pores are generated through the $ATPNa_2$ used as an organic phosphorus source to obtain HAp NRs. In our typical synthesis, $ATPNa_2$ molecules hydrolyze to release phosphate (PO_4^{3-}) ions and it was slowly react with Ca^{2+} ions via electrovalent bonds to be formed HAp nuclei with smaller aggregation. This smaller aggregation of HAp nuclei causes to prevent the agglomeration of the HAp NRs, resulting finer and uniform rods like morphology with higher SSA. The high encouraged for increasing the available electrochemical reactive sites.

3.3 Electrochemical properties

3.3.1 Electrochemical behaviour of Au/HAp nanocomposite modified GCE for hydrazine oxidation

The electrocatalytic activities of Au and Au/HAp nanocomposites were investigated towards the oxidation of hydrazine. This was performed with cyclic voltammetry (CVs) and amperometric (*i-t*) responses of rotating disc electrode (RDE)-based experiments, where a typical three electrode system consisting of a GCE modified with Au and Au/HAp nanocomposites was used as the working electrode. Scheme 2 illustrates the fabrication strategy of the Au/HAp/GCE toward the ultrasensitive hydrazine detection. The first step was the drop casting of Au/HAp nanocomposites on the bare GCE. The second step consists of two processes: (i) effective adsorption of hydrazine onto the catalytic surfaces due to electrostatic interaction between HAp and hydrazine and (ii) hydrazine can then be effectively dissociated/oxidized by Au NPs. Mechanism for the hydrazine oxidation in aqueous solutions can be established to be a four-electron transfer process to form N_2 and H^+ which can then react with OH^- to form water as shown in Eq.2.

$$N_2H_4^+ \rightarrow N_2 + 4H^+ + 4e^- \quad (2)$$

In order to investigate the electrocatalytic hydrazine oxidation, the CVs response were studied in the presence or absence of 2 µM of hydrazine with Au/HAp/GCE, Au/GCE, blank measurement at Au/HAp/GCE, blank measurement at Au/GCE and bare GCE as shown in Figure 8a-e. Curves a and b show the CVs response for the oxidation of hydrazine at Au/HAp/GCE and Au/GCE, respectively, with the presence of 2 µM of hydrazine. The oxidation current of hydrazine at Au/HAp/GCE is larger with a peak potential of 0.32 V. The Au/GCE exhibits a significantly higher over potential of 0.47 V for the hydrazine oxidation with smaller peak current. Therefore, the oxidation peak current of hydrazine at Au/HAp/GCE was much higher than that of Au/GCE with a peak to peak separation of 270 mV.

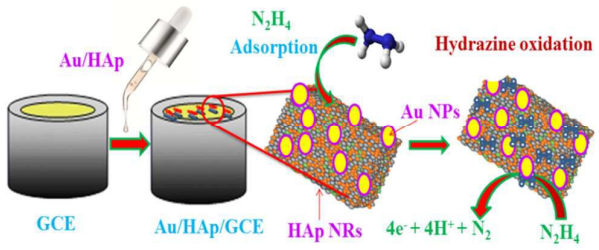

Scheme. 2 A schematic view of the Au/HAp/GCE toward ultrasensitive hydrazine detection.

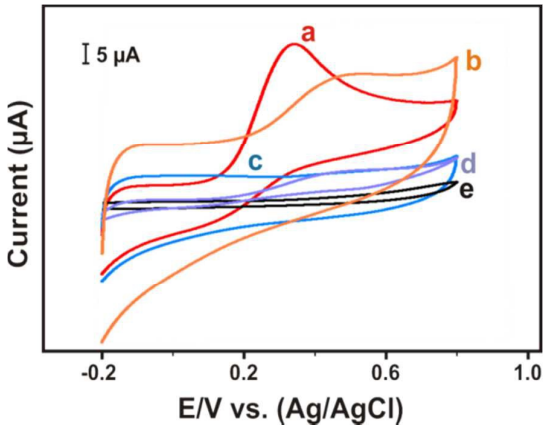

Fig. 8 CVs of 2 μM hydrazine in 0.1 M PBS on the Au/HAp/GCE (curve a), Au/GCE (curve b), blank measurement at Au/HAp/GCE (curve c), blank measurement at Au/GCE (curve d) and (curve e) bare GCE. Scan rate: 50 mV/s.

As can be seen the results that the electrochemical oxidation of hydrazine by Au/GCE is kinetically slow and a quite high overpotential is required at electrodes, which is not suited for quantification via conventional electrochemical methods. The Au/HAp/GCE exhibits a well-defined oxidation peak of hydrazine at 0.32 V, accompanied by a much lower oxidation onset potential and higher oxidation current. The lower onset potential specified that the electrocatalytic activity of Au/HAp/GCE nanocomposites is much stronger than that of Au/GCE. The increase in the oxidation current increases the rate of electron transfer to enhance electrocatalytic activity. Moreover, no oxidation peak current was observed with Au/HAp/GCE (curve c) and Au/GCE (curve d) with the absence of hydrazine. Curve e shows the oxidation of hydrazine at bare GCE. It requires a higher over potential and there was no observed obvious oxidation peak as shown in Figure 8.

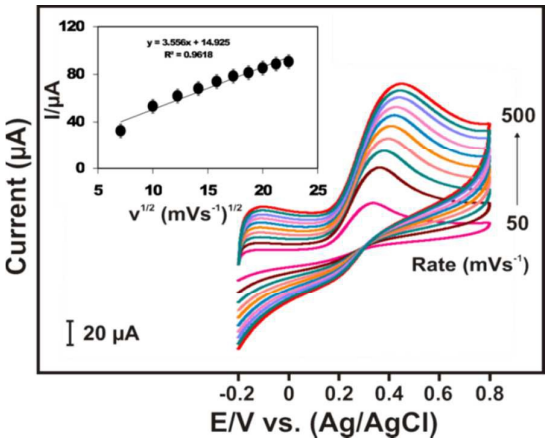

Fig. 9 (a) The CVs obtained at Au/HAp modified GCE in PBS (pH 7) containing 5 μM hydrazine at different scan rates (50–500 mV s^{-1}). Inset: The corresponding linear plot for the square root of scan rates vs I_p of hydrazine.

3.3.2 Effect of scan rate on hydrazine oxidation

The influence of scan rates on the anodic peak current was also studied in the range of 50-500 mV s^{-1} using 5 μM hydrazine in PBS (pH 7). The CVs responses of Au/HAp/GCE in Figure 9 clearly show the oxidation peak current (I_{pa}) increases with the increasing scan rates and the peak potentials were shifted towards a positive direction. This result indicates that the oxidation of hydrazine on the modified electrodes is an irreversible process. The inset in Figure 9 shows the linear relationship between the anodic peak current (I_{pa}) and the square root of scan rate ($v^{1/2}$) demonstrates the oxidation of hydrazine on Au/HAp/GCE is a diffusion-limited process. Furthermore, a linear relationship is also obtained between E_p and natural logarithm of scan rate (log v) for the electrode. The irreversible diffusive process, I_{pa} can be expressed as follows,

$$I_{pa} = 3.01\times10^{5} n[(1-\alpha)n_{\alpha}]^{1/2} AcD^{1/2}v^{1/2} \qquad (3)$$

Where α is the electron transfer coefficient, n_{α} is the electron number in the rate determining step, n is the total number of electrons involved in the oxidation of hydrazine, and other symbols have their usual meanings. The calculated slope of I_{pa} vs. $v^{½}$ is 0.8510, considering $(1-\alpha)n_{\alpha}$ = 0.45, D =1.2×10^{-6}cm^2/s and A = 0.10 cm^2, (estimated using Randles-Sevcik equation from the slope of peak currents of soluble 1 mM ferrocyanide in 0.1 M KCl vs. $v^{1/2}$). The estimated number of electrons involved in the anodic oxidation of hydrazine is about four-electron (n=4) on Au/HAp/GCE.

3.3.3 Effect of concentration on hydrazine oxidation

Figure 10 shows the CVs responses of Au/HAp/GCE in the presence of various concentrations of hydrazine (0.5 to 185 μM) in PBS (pH 7) at a fixed potential with the scan rate of 50 mV s^{-1}. It shows the oxidation peak current increases linearly with increasing the hydrazine concentration.

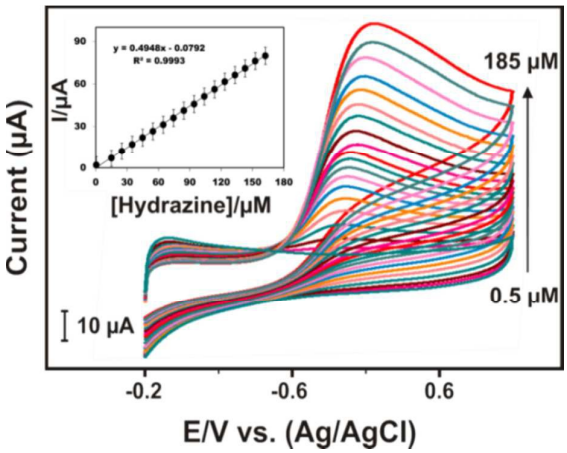

Fig. 10 CV responses of Au/HAp/GCE at 0.5-185 μM of hydrazine and Inset: The corresponding calibration plot for hydrazine concentration *vs* I_{pa}.

The linear regression equation was I_{pa} (μA) =0.4948x – 0.0792 with correlation coefficient of R^2 = 0.9996, where x is concentration of hydrazine as shown in the inset of Figure 10. The sensitivity was calculated from the slope of the calibration curve. The lower limit of detection and sensitivity was found to be 0.03 μM and 0.2177 μA $\mu M^{-1}cm^{-2}$. The obtained sensitivity can be attributed to the low charge transfer resistance of the Au/HAp/GCE and also the efficiency of the electron-transfer between hydrazine due to the catalytic effect and Au/HAp/GCE. The lower detection limit can be calculated by the following equation (3)

$$LOD = \frac{3S_B}{b} \qquad (3)$$

Where S_B is the standard deviation of the blank signal and b is the sensitivity. The obtained limits of quantification and detection for hydrazine sensing are much lower than that of the previously reported values for the other nanomaterials modified carbon-based electrodes[10,31&34] as show in Table 1. Significance of this study provided a clear evidence for the higher electrocatalytic activity of Au/HAp/GCE. Basically, HAp as a good adsorbent to adsorb all quantities of hydrazine and then the adsorbed hydrazine was effectively oxidized by Au NPs which leads to offer the enormous best electrocatalytic ability toward the sensing of hydrazine. Therefore, we found that the Au/HAp/GCE is more suitable high performance electrode for the electrochemical oxidation of hydrazine sensor.

3.3.4 Amperometric determination of hydrazine

In order to estimate the linear response range, sensitivity and detection limit for the amperometric (*i-t*) detection of ultratrace levels of hydrazine were recorded for Au/HAp nanocomposite modified electrode at various concentrations of hydrazine. The amperometric hydrazine detection was performed with a rotating disc electrode (RDE) at an applied potential of 0.2 V and the rotation speed was 900 rpm. Figure 11a shows the typical *i-t* responses of Au/HAp-based hydrazine sensor, the oxidation current increases linearly and then quickly with the successive addition of 0.5 μM hydrazine into the PBS, signifying a rapid and sensitive response upon the hydrazine concentration variation (0.5 to 1500 μM). When an aliquot of hydrazine was added into the stirred 0.1 M PBS (pH 7) solution, the amperometric responses achieved steady state within 2 seconds, which is fast amperometric behavior. A sharp and fast amperometric response was observed for each addition of 0.5 μM hydrazine, indicating the rapid diffusion of hydrazine on the Au/HAp modified rotating disc electrode surface. As a comparison, current response obtained at the Au/HAp electrode was much smaller than that obtained at the various electrodes, such as Au/AC,[10] Au/NH2-MIL-125 (Ti),[35] ZnO nanorods,[37] TiO_2NFs/GCE and TiO2–Pt,[39] which indicates the superb catalytic ability of Au/HAp nanocomposites. The rod-like HAp not only provided a suitable platform for the dispersion of Au NPs and enlarged specific surface area, but also favored the adsorption of hydrazine, thus bringing hydrazine closer to the catalytic sites of Au NPs and then increasing the efficiency of hydrazine oxidation. The analytical characteristics of Au/HAp electrode such as the linear range, sensitivity, and the limit of detection were calculated. The inset in Figure 11a shows that the oxidation current was linear with the hydrazine concentration in the range of 0.5-1429 μM. The linear regression value for the responses as I (μA) = 0.0321x + 0.128 with the correlation coefficient of R^2=0.9979, where x is the concentration of the hydrazine. The sensitivity of the proposed modified electrode was 0.05 μA μmM^{-1}. The limit of detection (LOD) was evaluated to be 0.017 μM by using Eqn (3) and the analytical performances of already reported hydrazine sensors are summarized in Table 1.

3.3.5 Selectivity, stability, repeatability and reproducibility studies

In order to evaluate the selectivity of Au/HAp/GCE for the sensing of hydrazine, we also investigated the influences of several potential interfering ions in the electrochemical experiments.

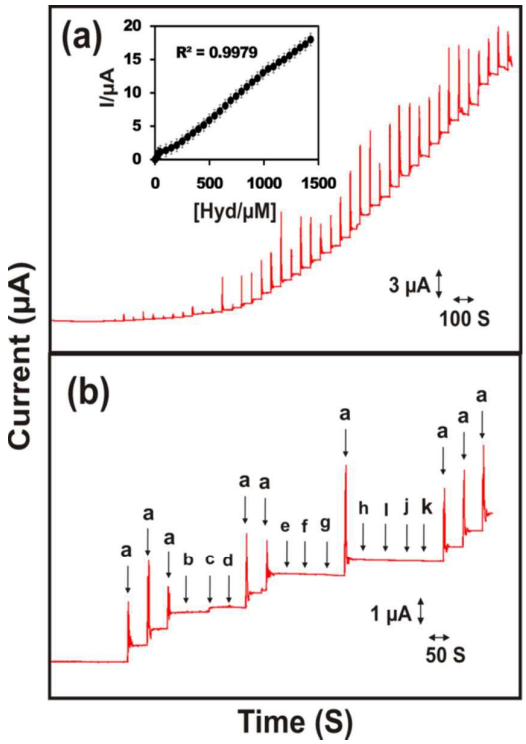

Fig. 11 (a) Amperometric i-t responses of Au/HAp modified rotating disc electrode at different concentrations of hydrazine in PBS (pH 7) at the rotation speed of 900 rpm. E_{app}= + 0.2 V. Inset: calibration plot for hydrazine [μM] vs. I_{pa}. (b) Amperometric i-t response at Au/HAp modified rotating disc electrode at different concentrations of 5 μM hydrazine (a), in the presence of 50 fold excess concentration of ascorbic acid (b), dopamine (c), uric acid (d), and in presence of 500 folds excess concentrations of $ZnCl_2$ (e), $CoNO_3$ (f), $NiCl_2$, (g) $CaCl_2$ (h), Na_2SO_3 (i) and KCl (j).

Table 1. Analytical parameters of the Au/HAp modified towards nitrite sensor comparison with previously reported similar modified electrodes

Glassy carbon modified electrode	Techniques	Limit of detection (μM)	Linear response range(μM)	Sensitivity ($\mu A \mu M^{-1} cm^{-2}$)	Ref.
Au/Hap NRs	*i-t* CV	0.017 0.03	0.5-14293 120	0.05 0.2177	**our work**
Au/AC	*i-t*	-	100 - 12000	0.16	10
Au/PPy/GCE	CV	0.2	1-500	0.126	35
Au/NH_2-MIL-125(Ti)	*i-t*	0.05	0.10-100	-	36
ZnO NRs	*i-t*	59.175	0.1 – 60	0.386	37
Nano-Au/porous-TiO_2	CV	0.5	2.5 – 500	_	38
TiO_2NFs/GCE	*i-t*	0.16	0.1-103	4.62	39

Table 2. Determination of hydrazine in various real samples

Samples	Analyte	Added (μM)	Found (μM)	Recovery (%)
Lake water	hydrazine	50 100	49.4 100	98.8 100
River water	hydrazine	50 100	48.8 100	97.6 100
Tap water	hydrazine	50 100	50 100	100 100

In the case of 0.5 μM hydrazine in PBS (pH 7.4) shows an insignificant interference for the 50-fold excess concentration of ascorbic acid, dopamine, uric acid, and in the presence of 500-folds excess concentrations of $ZnCl_2$, $CoNO_3$, $NiCl_2$, $CaCl_2$, Na_2SO_3 and KCl as shown in Figure 11b. This result indicates the proposed Au/HAp/GCE exhibit good anti-interference capability toward the detection of hydrazine. The storage stability of the reported hydrazine sensor was investigated in 0.5 μM hydrazine in N_2 saturated PBS (pH 7), and its oxidation peak current response was observed periodically. The proposed hydrazine sensor retains 91.17 % of its initial oxidation peak current response after 10 days in atmospheric air at room temperature indicates the good storage stability of the sensor. In order to observe the repeatability and reproducibility, we have prepared 5 different electrodes separately for the determination of 0.5 μM hydrazine and all the electrodes shows a high reproducibility. The relative standard deviation (RSD) of 1.7 % is observed from measurement of anodic peak currents. In addition, the repeatability for 10 successive measurements with the RSD of 2.6 % for the determination of 0.5 μM hydrazine indicates a good repeatability of the proposed sensor. Thus, the Au/HAp/GCE modified GCE shows good reproducibility throughout the detection of hydrazine.

3.3.6 Real sample analysis

In order to explore the real time applications of the sensor towards the determination of hydrazine, water samples collected from tap, lake and river have been employed for the real sample analysis. The results are shown in Table 2 and the recoveries ranged between 97.6 and 100%. The significant recoveries achieved in various water samples for the determination of trace level hydrazine reveals the practicality of the sensor towards hydrazine.

4. Conclusions

In summary, we have developed well-designed Au particles on HAp rods nanoarchitectures as a high performance electrocatalysts toward the oxidation of hydrazine from various water sources. Adenosine 5'-triphosphate disodium salt (Na_2ATP) as the phosphorus source was used to prepare HAp NRs through hydrothermal method at 180 ^oC for 12 h and negatively charged gold NPs solution was prepared by the citrate reduction of $HAuCl_4$. The precipitated citrate-stabilized Au NPs of 6-8 nm size were strongly anchored onto rod-shaped HAp with a diameter of ~ 10 nm and length of 60-65 nm. The physico-chemical properties, SSA and pore size distribution of Au/HAp nanocomposites were studied by using various analytical techniques. Based on the experimental results, we proposed nucleation growth mechanism for the nanoarchitectures. The Au/HAp nanocomposite shows excellent sensitive and selective determination of hydrazine sensors by using cyclic voltammograms (CVs) and amperometric (*i-t*) technique. Significant improvement in the hydrazine electrooxidation was achieved with the incorporation of Au NPs into HAp NRs, demonstrated by a wider linear range, a higher sensitivity and a lower limit of detection. The amperometric (*i-t*) responses reached steady state signals within 2 seconds, which is fast amperometric behavior. Furthermore, the present hydrazine sensor could be used repeatedly for the consecutive detection of hydrazine with high selectivity, good reusability and storage stability. The practical usefulness of the present hydrazine sensor was also proved in various real samples such as tap, lake and river water.

5. Acknowledgments

This work was supported by the Internal Research Grant, Alfaisal University (IRG 2014) project No. 4050101011410. The authors gratefully acknowledge the continued support from Alfaisal University and its office of Research.

6. References

1 L. Wei, H. Anne-Kristin, C. B. Nadja, R. Paramaconi, W. Dan, O. Mehtap, J. S. Thomas, N. Gaponik and A. Eychmüller, *Acc. Chem. Res*. 2015, **48**, 154–162.
2 W. C Christopher, J. H. Richard and T. T. David. *Appl.Catal.A*. 2005, **291**, 253
3 J. Chun-Jiang, L. Yong, B. Hans and S. Ferdi. *J. Am. Chem. Soc*. 2010, **132**, 1520–1522
4 C. Hong, Y. Weiying, L. Xiangjun, Z. Hong and Y. Zhuobin. *Anal. Methods*, 2012, **4**, 4176-4181
5 J. Zhang, X. Liu, L. Wang, T. Yang, X. Guo, S. Wu, S. Wang, and S. Zhang, J. Phys. Chem. C. 2011, 115, 5352–5357.
6 X. Liu, J. Zhang, L. Wang, T. Yang, X. Guo, S. Wu and S. Wang, J. Mater. Chem., 2011, 21, 349–356.
7 H. Wenjing, B. Hua, X. Yuxi, Y. Zhiyi, G. Zhongze and S. Gaoquan. *J. Phys. Chem. C*. 2010, **114 (4)**, 1822–1826
8 A. Randa, G. Nébéwia, L. Aazdine, F. Nordin, M.C. Mohamed and M. Claire. *Chem. Mater*. 2015, **27 (16)**, 5464–5478
9 S. Guangyu, C. Chenbo and Y. Jifeng. *Electrochimica Acta*. 2011, **56**, 8272–8277
10 M. Rajesh, V. Vediyappan and C. Shen-Ming. *Sensors and Actuators B: Chemical*. 2014, **204**, 382-387.
11 C. Zhang, C. Li, S. Huang, Z. Hou, Z. Cheng, P. Yang, C. Peng and J. Lin. *Biomaterials*. 2010, **31**, 3374–3383.
12 A. Naldoni, A. Minguzzi, A. Vertova, V. Dal Santo, B. Laura and L.B. Claudia. *J. Mater. Chem*. 2011, **21**, 400–407.
13 G. Bharath and N. Ponpandian. *RSC Adv*. 2015, **5**, 84685-84693.
14 Z. Ying, Z. Wei, Z. Qing, L. Kaiyang, L. Wei, L. Yong and E.B. Craig. *Analyst*, 2014, **139**, 5362
15 P. Kanchana and C. Sekar. *Materials Science and Engineering: C*, 2014, **42**, 601-607.
16 Y. Huanshun, Z. Yunlei, A. Shiyun, L. Xianggang, Z. Lusheng and L. Linan. *Microchim Acta*. 2010, **169**, 87–92
17 P. Kanchana, N. Lavanya and C. Sekar. *Materials Science and Engineering: C*, 2014, **35**, 85-91
18 H. Y. Zhao, X. X. Xu, J. X. Zhang, W. Zheng and Y. F. Zheng. *Bioelectrochemistry*, 2010, **78**, 124–129
19 G. Bharath, M. Rajesh, C. Shen-Ming, V. Vediyappan, A. Balamurugan, D. Mangalaraj, C. Viswanathan and N. Ponpandian, *J. Mater. Chem. B*, 2015, **3**, 1360-1370
20 G. Bharath, A. Jagadeesh Kumar, K. Karthick, D. Mangalaraj, C. Viswanathan and N. Ponpandian. *RSC Adv*., 2014, **4**, 37446-37457.
21 G. Bharath, D. Prabhu, D. Mangalaraj, C. Viswanathan and N. Ponpandian. *RSC Adv*. 2014, **4**, 50510-50520.
22 Q. Chao, Z. Ying-Jie, Z. Xin-Yu, L. Bing-Qiang, T. Qi-Li, Z. Jing and C. Feng. *Chem. Eur. J*. 2013, **19**, 981 – 987.
23 Q. Chao, T. Qi-Li, Z. Ying-Jie, Z. Xin-Yu and C. Feng. *Materials Letters*, 2012, **85**, 71–73.
24 C. Huaqiang, Z. Lu, Z. He and W.J. Zhao. *Phys. Chem. C*, 2010, **114**, 18352–18357
25 Z. Xin-Yu, Z. Ying-Jie, C. Feng, L. Bing-Qiang, Q. Chao, Z. Jing and W. Jin. *CrystEngComm*, 2013, **15**, 7926-7935
26 Q. Chao, Z. Ying-Jie, Z. Yong-Gang, J. Ying-Ying, W. Jin and C. Feng. *J. Mater. Chem. B*, 2015, **3**, 7347-7354
27 Y. Juan, D. Weiping, D. Shijia and J. Huangxian. *Electroanalysis*. 2009, **21**, 190 -195.
28 S. Hao, S. Fang-Zheng, N. Ji, C. Yong, H. He-Yong and F. Kang-Nian. *Angew. Chem. Int. Ed*. 2009, **48**, 4390-4393.
29 S. Guangyu, C. Chenbo and Y. Jifeng. *Electrochimica Acta*. 2011, **56**, 8272–8277.
30 Z. Kunfeng, Q. Botao, W. Junhu, Z. Yanjie and Z. Tao, *Chem. Commun*. 2011, **47**, 1779–1781.
31 K. Atiweena, S. Pattarachai, L. Santamon and S. Montree. *Anal. Chem*. 2014, **86**, 12272−12278
32 G. Xin and P.C. Jon. *Anal. Chem*. 2015, **87**, 6460-6464.
33 H. Yaping, Z. Jianbin and S. Qinglin. *Microchim Acta*. 2012, **177**, 479–484
34 A. Naldonia, M. D'Arienzob, A. Marco, M. Marcello, S. Roberto, M. Franca, S. Elena and D. S. Vladimiro. *Appl. Catal., B*. 2013, **130**, 239–248.
35 L. Jing and L. Xiangqin. *Sensors and Actuators B*, 2007, **126**, 527–535.
36 H. Yujie, H. Lei, Z. Lingling and D. Shaojun. *J. Mater. Chem. A*. 2015, **3**, 14669-14674
37 A. Rafiq, T. Nirmalya, J. Da-Un-Jin and H. Yoon-Bong. *Chem. Commun*. 2014, **50**, 1890.
38 G. F. Wang, C. H. Zhang, X.P. He, Z.J. Li, X.J. Zhang, L. Wang and B. Fang. *Electrochim. Acta*, 2010, **55**, 7204.
39 D. Yu, W. Ying, Z. Lichun, Z. Heng, M.L. Chang and L. Yu. *Nanoscale*, 2011, **3**, 1149.